



Research
Glycomedicine—Article

Ablation of *ST6Gal-I* Downregulates BACE1 Expression and Suppresses Production of A β ₄₂ Plaques in Alzheimer's Disease



Kangkang Yang^{a,b,#}, Xueying Li^{c,#}, Minchao Lai^{d,#}, Weiwei Zhao^e, Wanli Song^{e,f}, Shaobin Chen^a, Wenzhe Li^{a,e,f,*}

^a Department of Thoracic Surgery, Cancer Hospital of Shantou University Medical College, Shantou 515041, China

^b Institute for Genome Engineered Animal Models of Human Diseases, National Center of Genetically Engineered Animal Models for International Research, Liaoning Province Key Lab of Genetically Engineered Animal Models, Dalian Medical University, Dalian 116044, China

^c Department of Virology, Research Institute for Microbial Diseases, Osaka University, Osaka 565-0871, Japan

^d Department of Neurology, The First Affiliated Hospital of Shantou University Medical College, Shantou 515041, China

^e Chaoshan Branch of State Key Laboratory of Esophageal Cancer Prevention and Treatment & Shantou Key Laboratory of Glycoconjugates for Immunodiagnosis and Immunotherapy, Shantou University Medical College, Shantou 515041, China

^f Institute for Glycome Study, Shantou University Medical College, Shantou 515041, China

ARTICLE INFO

Article history:

Received 21 September 2024

Revised 18 January 2025

Accepted 24 February 2025

Available online 7 March 2025

Keywords:

α 2,6-Sialyltransferase-1

Sialylation

β -Site amyloid precursor protein cleaving enzyme 1

Amyloid- β ₄₂

Alzheimer's disease

ABSTRACT

Recent studies indicate the involvement of glycosylation in the pathogenesis of Alzheimer's disease (AD). α 2,6-Sialylation, catalyzed by α 2,6-sialyltransferase-1 (ST6Gal-I), corresponds to the development of the infant brain and nervous system, however the mechanism of aberrant α 2,6-sialylation affects multiple physiological and pathological conditions remains unclear. The present study, *in vitro* and *in vivo*, showed that expression of ST6Gal-I and α 2,6-sialylation levels were up-regulated in cerebrospinal fluid and sera of AD patients. In addition, levels of α 2,6-sialylation were also increased in brain and sera of AD model mice. Furthermore, deletion of *ST6Gal-I* reduced β -site amyloid precursor protein cleaving enzyme 1 (BACE1) levels and alleviated the impairment of learning and memory induced by scopolamine in rats. BACE1, a hyper-sialylated protein, plays a critical role in amyloid- β ₄₂ (A β ₄₂) production. *ST6Gal-I* knock-down in Neuro-2a neuroblastoma cells (*ST6Gal-I*-KD-N2a) reduced the expression of BACE1 via promoting its ubiquitination. Deletion of *ST6Gal-I* suppressed amyloid precursor protein (APP) cleaved by BACE1, followed by a decrease in A β ₄₂ production, while alleviated A β ₄₂-induced apoptosis. This study first reveals a significant role of α 2,6-sialylation in development and progression of AD, suggesting that ST6Gal-I is a novel glycan therapeutic target for AD diagnosis and treatment.

© 2025 THE AUTHORS. Published by Elsevier LTD on behalf of Chinese Academy of Engineering and Higher Education Press Limited Company. This is an open access article under the CC BY-NC-ND license (<http://creativecommons.org/licenses/by-nc-nd/4.0/>).

1. Introduction

Alzheimer's disease (AD) is a form of neurodegeneration distinguished by a gradual erosion of memory and cognitive functions, and it stands as the predominant cause of dementia among the elderly [1]. The "amyloidogenic hypothesis" in AD posits that the aggregation of amyloid- β (A β) plaques serves as a pathological catalyst [2]. A β peptides are generated by sequential enzymatic processing of amyloid precursor protein (APP) by β -site amyloid precursor protein cleaving enzyme 1 (BACE1) and γ -secretase,

resulting in the formation of characteristic plaques in the brains of patients [3]. BACE1, a type I transmembrane protein, plays a crucial role as key enzyme in A β peptide biosynthesis during AD pathogenesis [4]. For example, the enzymatic activity and protein expression of BACE1 are correlated with A β plaque numbers and cognitive status [5]. *BACE1* and *APP* double-transgenic mice show enhanced A β generation and exacerbated A β pathology [6]. Conversely, there are no A β plaques or memory deficits in *BACE1*-deficient 5XFAD mice [7].

Glycosylation is a post-translational modification characterized by the addition of oligosaccharides to proteins in endoplasmic reticulum (ER)/Golgi secretory pathway, by glycosidases and glycosyltransferases (Fig. 1(a)). The ecto-domain of BACE1 contains four glycosylated asparagine sites at N¹⁵³, N¹⁷², N²²³, and N³⁵⁴.

* Corresponding author.

E-mail address: liwenzhe@stu.edu.cn (W. Li).

These authors contributed equally to this work.

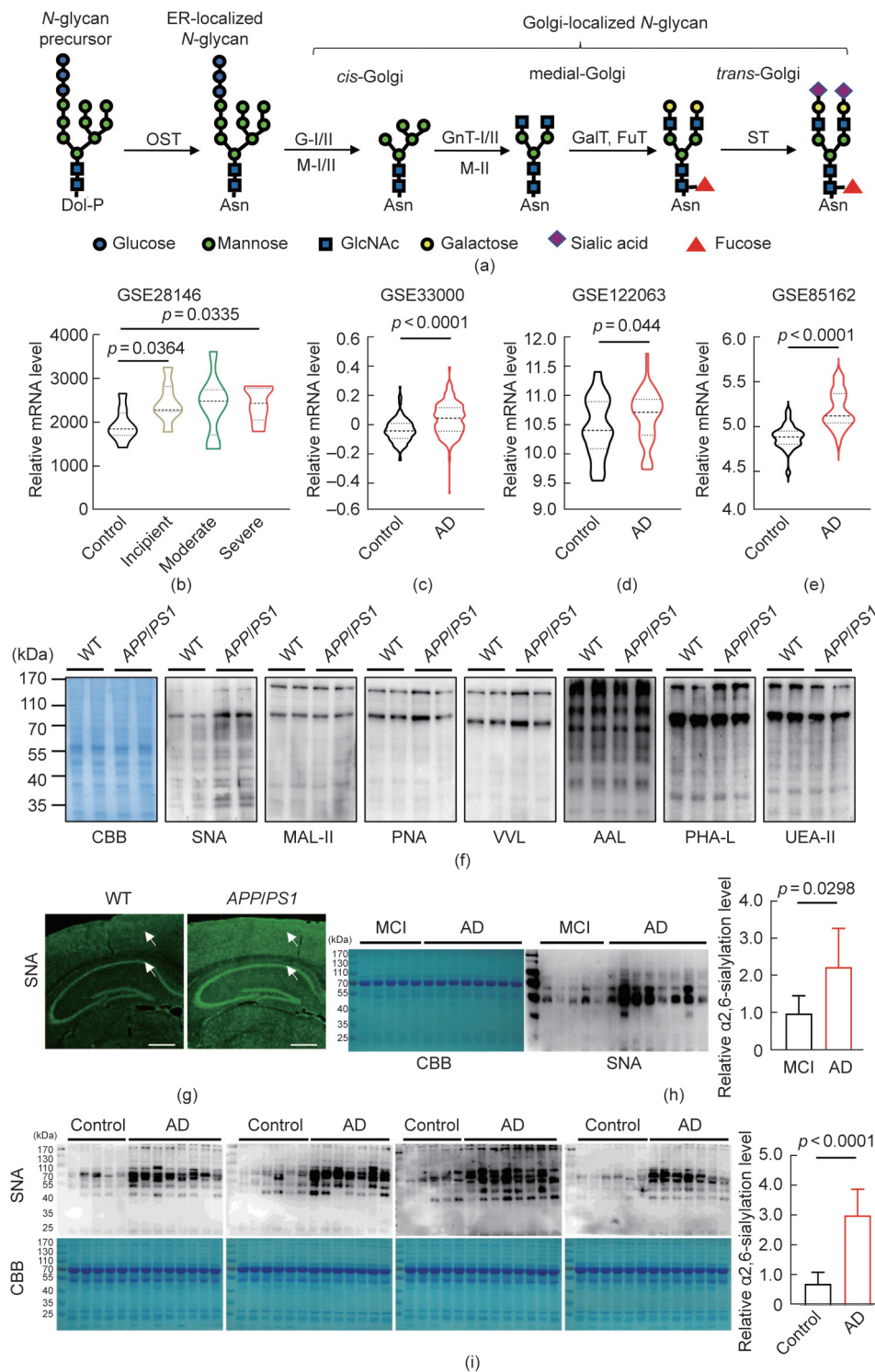


Fig. 1. $\alpha 2,6$ -Sialylation is increased in AD serum and brain tissue. (a) Simplified schematic of the N-glycan synthesis in mammalian cells. Shown are the different classes of N-glycans catalyzed by several glycosidases and glycosyltransferases, such as oligosaccharyltransferase (OST), α -glucosidases I/II (G-I/II), α -mannosidase I/II (M-I/II), N-acetylglucosaminyltransferase I/II (GnT-I/II), galactosyltransferases (GalT), fucosyltransferase (FuT), and sialyltransferase (ST). The OST transfers the 14-sugar glycan (Glc3Man9GlcNAc2) from dolichol phosphate (Dol-P) to the asparagine (Asn) in an Asn-X-serine (Ser)/threonine (Thr) motif. While this figure depicts events in a particular order, it must also be noted that the pathway is more flexible than shown and some of the enzymes can act in different order. GlcNAc: saccharide N-acetylglucosamine. (b) Compare expression of ST6Gal-I in the brain tissues of AD patients at different stages (incipient, $n = 7$; moderate, $n = 8$; severe, $n = 7$) with controls ($n = 8$) in the GSE28146 database. (c) Expression of ST6Gal-I in the brain tissues of AD ($n = 310$) patients compared with controls ($n = 157$) in GSE33000. (d) Expression of ST6Gal-I in the brain tissues of AD ($n = 56$) patients compared with controls ($n = 44$) in GSE122063. (e) Expression of ST6Gal-I in the brain tissues (prefrontal cortex (Cor) and hippocampus (Hip)) of APP/PS1-AD mice compared with controls ($n = 29$) in GSE85162. (f) Lectin blots. Hip samples (5 μg) of APP/PS1-AD mice were characterized by lectin blots with *Sambucus nigra* agglutinin (SNA), *Maackia amurensis* lectin-II (MAL-II), peanut agglutinin (PNA), *Vicia villosa* lectin (VVL), *Aleuria aurantia* lectin (AAL), *Phaseolus vulgaris* lectin-L (PHA-L), and *Ulex europaeus* lectin-II (UEA-II) (1:10 000). Wild-type (WT) and APP/PS1, $n = 6$. (g) Immunofluorescence assay. Brain tissues from APP/PS1 mice were stained with SNA (1:100). WT and APP/PS1, $n = 6$, scale bar = 500 μm . (h) SNA blots of the CSF of AD patients. $\alpha 2,6$ -Sialylation levels in CSF samples (10 μg) of AD patients ($n = 8$) and MCI ($n = 5$) were characterized by probing with SNA (1:10 000). (i) SNA blots of the sera of AD patients. $\alpha 2,6$ -Sialylation levels in serum samples (2.5 μg) of AD patients ($n = 30$) and age-matched healthy controls ($n = 22$) were characterized by probing with SNA (1:10 000). Data were presented as the means \pm standard deviation (SD). $p < 0.05$ was considered statistically significant.

The activity of BACE1 is modulated by the degree of N-glycosylation [8]. The α 2,6-sialyltransferase-I (ST6Gal-I) transfers sialic acid (*N*-acetylneuraminic acid) from a cytidine-5'-monophosphate-*N*-acyl-neuraminic acid donor to the terminal galactose residue on the *N*-glycans of glycoproteins via α 2,6-linkage (α 2,6-sialylation) [9]. Sialylation is an important parameter in protein folding, structural stability, enzymatic activity, and molecular sorting [10,11]. Whereas, the pathophysiological significance of α 2,6-sialylation in the context of AD remains largely elusive.

To investigate ST6Gal-I function during AD occurrence, we established a *ST6Gal-I*-deficient (*ST6Gal-I*^{-/-}) rat model by clustered regularly interspaced short palindromic repeats (CRISPR)/CRISPR-associated protein 9 (Cas9) gene editing. Scopolamine (Scop)-induced memory impairment was suppressed in brains of *ST6Gal-I*^{-/-} rats. The cleavage of APP by BACE1 and the subsequent formation of A β ₄₂ were also found to be reduced in Neuro-2a neuroblastoma cells with *ST6Gal-I* knockdown (*ST6Gal-I*-KD-N2a). Notably, both ST6Gal-I and α 2,6-sialylation are elevated in brains and sera of AD patients, as well as in AD model mice. These findings implicate ST6Gal-I may as a promising therapeutic target for interventions aimed at ameliorating AD pathogenesis.

2. Materials and methods

2.1. Clinical samples

Serum samples from a total of 52 AD patients and 38 healthy controls were collected. Cerebrospinal fluid (CSF) samples were collected from five mild cognitive impairment (MCI, mean age 75 years) patients and eight AD patients (mean age 78 years). All control, MCI, and AD patients were diagnosed in department of neurology of the First Affiliated Hospital of Shantou University Medical College. All clinical experiments were approved by the Ethics Committee of the First Affiliated Hospital of Shantou University Medical College (No. B-2023-017). AD transcriptome data were obtained from the Gene Expression Omnibus (GEO) database (Table S1 in Appendix A).

2.2. Antibodies

Antibodies used were anti-APP (76600s), anti-BACE1 (D10E5), and anti-Flag tag (14793) from Cell Signaling Technology (USA); anti-BACE1 (12807-1-AP), anti-caspase 3 (19677-1-AP), and anti-glyceraldehyde-3-phosphate dehydrogenase (GAPDH; 1E6D9) from Proteintech (China); anti-soluble APP beta (sAPP β ; 18957) and anti-ST6Gal-I (28047) from Immuno-Biological Laboratories (Japan); Alexa Fluor 488-conjugated mouse anti-GM130 (560257) from BD Biosciences (USA); anti-Bad (610391), anti-Bcl-2 (610538), and anti-P53 (610183) from BD Transduction Laboratories (USA); anti-caspase 9 (BS1731) from Bioworld Technology (USA); horseradish peroxidase (HRP)-conjugated anti-mouse IgG (A0216), anti-rabbit IgG (A0208), streptavidin (A0303), Alexa Fluor 488-/350-labeled goat anti-rabbit IgG(H+L) (A0423/A0408), streptavidin/Alexa Fluor AF647 (K0068R-AF647), and streptavidin/Alexa Fluor AF488 (K0068R-AF488) from Beyotime Biotechnology (China).

2.3. Generation of the *ST6Gal-I* knockout rat

Our *ST6Gal-I* knockout (*ST6Gal-I*^{-/-}) rat model was generated using CRISPR/Cas9 technology. To target the *ST6Gal-I* gene, four guide RNAs (gRNAs), named 3358-*ST6Gal-I*-5S1, 3358-*ST6Gal-I*-3S1, 3358-*ST6Gal-I*-5S2, and 3358-*ST6Gal-I*-3S2, were designed (Table S2 in Appendix A). The gRNAs were precisely microinjected into the cytoplasm of fertilized pronuclear-stage rat ova, following

which the viable eggs were carefully implanted into the uterine cavities of pseudopregnant female rats. Subsequently, genetic profiling was conducted on DNA samples extracted from the tails of two-week-old F0 generation rats. Three *ST6Gal-I* heterozygous (*ST6Gal-I*^{+/-}) F0 generation rats (Table S3 in Appendix A) and a total of 22 rats (6 *ST6Gal-I*^{+/-} and 16 *ST6Gal-I*^{-/+}) F1 generation rats (Table S4 in Appendix A) were obtained. Offspring of F1 *ST6Gal-I*^{+/-} mating were used for all experiments described in this article. The genotypes were checked by polymerase chain reaction (PCR). The primers were 5'-TACAGACCTTGTGGAGTACGGAG-3' (forward), and 5'-CCTGGAGTGTCAAAGGACCAT-3' (reverse) for *ST6Gal-I*^{-/-} rats; 5'-TACAGACCTTGTGGAGTACGGAG-3' (forward) and 5'-TCTGCTCTCGCTCACTCAAGT-3' (reverse) for *ST6Gal-I*^{+/+} rats.

2.4. Scop-induced AD model

Scop hydro-bromide (Sigma-Aldrich, Germany; 2 mg·kg⁻¹) was administered to rats through the intraperitoneal route. *ST6Gal-I*^{+/+} and *ST6Gal-I*^{-/-} rats (230–250 g) were each randomly divided into a control group (intraperitoneally administered 0.9% saline, 2 mL·kg⁻¹·d⁻¹ for 21 d) or an experimental group (intraperitoneally administered Scop at a dose of 2 mg·kg⁻¹·d⁻¹ for 21 d). All animal procedures were approved by the Institutional Animal Care and Use Committee (IACUC) of Shantou University Medical College.

2.5. Behavioral experiments in rats

The Morris water maze (MWM) test was performed as previously described [12]. The duration in the platform quadrant, total distance and swimming speed were monitored by Any-maze (Global Biotech Inc., China). The nest-building test was adapted from published methods [13]. All results were scored blindly. The novel object recognition (NOR) test was performed according to published methods [14]. Data were collected using tracking software, and manual scoring was used to assess behavior from the videos. The discrimination index (DI) was calculated using the following equation: $DI = T_{\text{novel}} - T_{\text{familiar}} / (T_{\text{novel}} + T_{\text{familiar}})$ and preference index (PI) was calculated using the following equation: $PI = T_{\text{novel}} \text{ or } T_{\text{familiar}} / (T_{\text{novel}} + T_{\text{familiar}})$, where T_{novel} represents for the time rats spent exploring the novel object and T_{familiar} represents for the time rats spent exploring the familiar object.

2.6. Western and lectin blots

Equal protein samples were separated by sodium dodecyl sulfate-polyacrylamide gel electrophoresis and then transferred to polyvinylidene fluoride (PVDF) membranes (Millipore, USA). After incubation, the membranes were incubated with primary antibodies or biotin-labeled lectins, then, incubated with HRP-conjugated secondary antibody or streptavidin, and visualized with an electrochemiluminescence (ECL) system (Beyotime Biotechnology). The gel was stained with Coomassie brilliant blue (CBB) as a loading control. Data quantification was performed by ImageJ software.

2.7. Transfection of *ST6Gal-I* siRNA

N2a cells (5×10^4) were seeded in six-well plates. Three targeting sequences of the *ST6Gal-I* small interfering RNA (siRNA) used were as follows: siRNA-1 (828–848) (sense: 5'-CCACUGAAUGGGAGG-GUUATT-3', antisense: 3'-TTGGUGACUUACCCUCCAAU-5'); siRNA-2 (1495–1515) (sense: 5'-GGGAACAGAUGAAGACAUJTT-3', antisense: 3'-TTCCCUUGUCUACUUCUGUAA-5'); siRNA-3 (931–951) (sense: 5'-CCAGCUGGUGCGAGAGAUJTT-3', antisense: 3'-TTGGUCGACCCAGCUCUAA-5'); and control (sense: 5'-UUCUCCGAACGUGUCACGUTT-3', antisense: 3'-TTAAGAGGCUUGCACAGUGCA-5'). N2a cells were transfected with 100 pmol of control siRNA or *ST6Gal-I* siRNA, using 10 μ L of lipofectamine 3000 (L3000-015; Invitrogen, USA).

2.8. Establishment of ST6Gal-I knockdown and restored N2a cell lines

The pLKO.1 short hairpin RNA (shRNA) lentivirus system was used to generate shRNA virus against the *ST6Gal-I* gene (siRNA1; *ST6Gal-I*-shRNA, sense: 5'-TAATACGACTCACTATAGGG-3', anti-sense: 5'-CTGGAATAGCTCAGAGGC-3'). 293T cells at 80% confluence in a 10 cm dish were simultaneously transfected with 3.5 µg of the plasmid of regulator of expression of virion protein (pREV), 3.5 µg of the plasmid of group-specific antigen protein (pGag), 1.75 µg of the plasmid of vesicular stomatitis virus glycoprotein (pVSVG), and 3.5 µg of control or *ST6Gal-I*-shRNA, using 20 µL lipofectamine 3000. The virus particles were concentrated (10-fold) with polyethylene glycol (PEG) 8000 (Sangon Biotech, China). N2a cells were transduced with virus solution containing 6 µg·mL⁻¹ polybrene (Sigma-Aldrich). *ST6Gal-I* knockdown (*ST6Gal-I*-KD) cells were obtained by selection in 5 µg·mL⁻¹ puromycin (Beyotime Biotechnology).

To prepare *ST6Gal-I* restored cells, pEZ-M77-*ST6Gal-I*-His mutant expression vectors were prepared. The pEZ-M77-*ST6Gal-I*-His vector was transduced into *ST6Gal-I*^{-/-} cells by lipofectamine 3000, and positive *ST6Gal-I* cells (*ST6Gal-I*-KD-Re) were generated after selection in 300 µg·mL⁻¹ neomycin (AbMole, China).

2.9. Generation of BACE1-overexpressing N2a cells

BACE1-overexpressing (*BACE1*-OE) N2a cells were obtained by transfection of a recombinant pEZ-M35-*BACE1*-Flag vector with lipofectamine 3000 according to the manufacturer's instructions. At 48 h after transfection, the *BACE1*-OE N2a cells were selected in 300 µg·mL⁻¹ neomycin (AbMole).

2.10. Real-time quantitative polymerase chain reaction (RT-qPCR)

Total RNA from cultured cells was extracted using RNAiso Plus reagent (TaKaRa, China) according to the manufacturer's protocol. Briefly, total RNA (1 µg) was reverse transcribed using PrimeScript RT Master Mix (TaKaRa). For RT-qPCR, complementary DNA (cDNA) was performed using SYBR Green Master Mix (TransGen Biotech, China) by an Applied Biosystems Prism 7000 Sequence Detection System (Japan). Relative fold changes of target genes amplification were calculated according to the 2^{-ΔΔCt} method. Primers used listed in Table S5 in Appendix A.

2.11. Enzyme-linked immunosorbent assay (ELISA)

BACE1 enzyme activity was measured with an ELISA kit (AMK, China) according to the manufacturer's protocol. The levels of Aβ₄₂ were quantified by using a sandwich ELISA kit (Elabscience Biotechnology, China).

The APP was immobilized onto a 96-well plate and incubated overnight at 4 °C. Subsequently, the wells were thoroughly rinsed and then sealed with 200 µL of bovine serum albumin (BSA), which was incubated at 37 °C for a period of 2 h. After washing, each well was treated with 100 µL of a binding buffer (phosphate-buffered saline (PBS), 0.05% Tween, and 1% BSA), supplemented with varying concentrations of purified *BACE1* protein, both α2,6-sialylated and de-α2,6-sialylated forms. This mixture was then incubated at 37 °C for 1 h. Then, 100 µL of HRP-conjugated secondary antibody was introduced to the wells, and the plate was incubated at 37 °C for 1 h. Thereafter, 100 µL of *o*-phenylenediamine was added to each well, and the plate was placed in a dark setting for a 20 min incubation at room temperature. The concentration of *BACE1* required to achieve 50% of the maximal binding effect (EC₅₀) was quantified by measuring the optical density at 492 nm using an ELISA reader (Thermo Fisher Scientific, USA).

2.12. RNA sequencing (RNA-seq)

Total RNA was isolated from *ST6Gal-I*-shRNA-control (shctl) and *ST6Gal-I*-KD cells using TRIzol reagent (Invitrogen), adhering to the supplier's instructions, for subsequent RNA-seq processing by Annoroad company (China). The process involved diluting the total RNA in a buffer and proceeding through a series of steps: reverse transcription, pre-amplification, purification of cDNA, and the creation of circular single-stranded DNA (ssDNA) libraries. During PCR, each library was assigned a unique barcode and subsequently sequenced on a BGISEQ500 platform, utilizing 100-base pair single-end reads.

2.13. Immunoprecipitation (IP)

Protein lysate (1 mg) was incubated with the specified antibodies (5 µL) overnight under gentle shaking conditions. After wash, 30 µL protein G-Sepharose (Sangon Biotech) was added to the mixture, followed by rotation. The bound proteins were boiled in 2× Laemmli sample buffer or eluted with Tris-HCl (pH = 2.5) buffer.

2.14. Immunofluorescence

After deparaffinized, hydrated, and blocked, rat brain tissue sections were incubated with primary antibodies, and then incubated with fluorescent secondary antibodies. Finally, the sections were examined under a fluorescence microscope (Leica, UK). Similarly, cells were fixed, permeabilized, blocked, and incubated with primary antibodies and fluorescent secondary antibodies. Fluorescence images were visualized using an A1R MP multiphoton confocal microscope (Nikon, Japan).

2.15. Chromatin immunoprecipitation (CHIP)

CHIP was performed using CHIP kit (Beyotime Biotechnology). Specifically, 1% formaldehyde was added to the cell culture to cross-link the protein with DNA fragments, and then the cells were broken up with ultrasound, breaking the chromatin into fragments. Then, anti-specificity protein 1 (SP1) antibody (ab227383; Abcam, UK) was added to the sample and rotated overnight at 4 °C. The DNA-protein complex was precipitated using protein agarose/sepharose and then centrifuged at 12 000g for 5 min. Finally, according to the instructions of SYBR Green Pro TaqHS QPCR Kit (Hunan Precision Biotechnology Co., LTD., China), the obtained precipitation was analyzed by fluorescence RT-qPCR technology. The primer sequence of *BACE1* gene promoter region was detected as follows: *BACE1* promoter forward: 5'-GCCACAAGTCTTTCCGCCTCC-CCAG-3'; *BACE1* promoter reverse: 5'-ACGGGAGCAGGGGAGAG-GCTGGGAT-3'.

2.16. Sample measurement using multiplexed capillary gel electrophoreses with laser induced fluorescence (xCGE-LIF) detection

N-glycan structures were detected using xCGE-LIF as published [15]. In brief, 2 µL of purified *N*-glycan and 8 µL of formamide mixture (containing 1 µL of GeneScan™ 500 LIZ™ size standard; Life Technologies, Germany) were added to a 96-well plate, and capillary gel electrophoresis was performed on a glucose tester with a sample running voltage of 15 kV and an electrophoresis time of 2200 s. Glycoder software was used to analyze the experimental results. The resulting abscissa is the peak time, and the ordinate is the resulting plot of fluorescence intensity. Peak area percentage (PAP) represents the peak area ratio.

2.17. Statistical analysis

Data are presented as mean \pm standard deviation (SD) from at least three repeated experiments. The GraphPad Prism (Version 9.0) was used for statistical analysis and difference comparison of experimental data. Two-tailed Student's *t*-tests were performed to compare the statistical differences between two groups. One-way analysis of variance (ANOVA) and two-way ANOVA were used between multiple groups to evaluate whether there were statistical differences between the groups. Differences with $p < 0.05$ were considered statistically significant.

3. Results

3.1. α 2,6-Sialylation is increased in AD patients

The altered glycosylation is commonly found in AD patients. To assess glycosylation in AD, we investigated the glycosyltransferases expression. The AD patients' datasets (GSE28146) were downloaded from GEO database. AD patients had higher expression of ST6Gal-I in brain tissues (Figs. S1(a) and S1(b) in Appendix A) and at different AD stages (incipient, moderate, and severe) (Fig. 1(b)). Consistently, the expression of ST6Gal-I was higher in brains of AD patients in the GSE33000 (Fig. 1(c)) and GSE122063 (Fig. 1(d)) datasets. The diagnostic ability of ST6Gal-I to predict AD progression was assessed using receiver operating characteristic (ROC) analysis. The area under the curve (AUC) for ROC curves were 0.801 ($p = 0.0129$), 0.722 ($p < 0.0001$), and 0.622 ($p = 0.0366$) for the GSE28146, GSE33000, and GSE122063 datasets, respectively (Fig. S1(c) in Appendix A). *APP/presenilin 1 (PS1)* double transgenic mice display accelerated A β deposition and reliable memory deficits in the brain [16]. Compared to wild-type (WT) mice group, the messenger RNA (mRNA) level of *ST6Gal-I* were obviously up-regulated in the brain of *APP/PS1* double transgenic mice, including prefrontal cortex (Cor) and hippocampus (Hip) tissues (Fig. 1(e), Figs. S1(d) and S1(e) in Appendix A) in GSE85162. In addition, we have also verified these results, which show that compared to WT mice, the levels of *ST6Gal-I* mRNA and protein in the Hip and prefrontal Cor of *APP/PS1* mice were both up-regulated (Figs. S2(a) and S2(b) in Appendix A). Furthermore, glycosylation levels in brains of *APP/PS1* mice were determined with lectin blots. Probing with *Sambucus nigra* agglutinin (SNA), which recognized for α 2,6-sialylation [9], SNA showed α 2,6-sialylation was increased in *APP/PS1* mice brain (Fig. 1(f)). However, there was no significant change in blots probed with the remaining lectins, such as *Maackia amurensis* lectin-II (MAL-II, specific for Sia α 2-3Gal/GalNAc), peanut agglutinin (PNA, specific for Gal β 1-3GalNAc-Ser/Ter), *Vicia villosa* lectin (VVL, specific for GalNAc α and GalNAc α 1-3Gal), *Aleuria aurentia* lectin (AAL, specific for fucose), *Phaseolus vulgaris* lectin-L (PHA-L, specific for Gal β 1-4GlcNAc β 1-2Man), and *Ulex europaeus* lectin-II (UEA-II, specific for GlcNAc β and Fuc α 1-2Gal β 1-4GlcNAc). In immunofluorescence staining, the levels of α 2,6-sialylation (Fig. 1(g)) and APP (Fig. S2(c) in Appendix A) were up-regulated in *APP/PS1* mice brains compared to WT mice.

We also evaluated α 2,6-sialylation in CSF from five MCI and eight AD patients by lectin blotting with SNA. Compared with MCI patients, α 2,6-sialylation was dramatically increased in CSF of AD patients (Fig. 1(h)). The α 2,6-sialylation was elevated in sera of AD patients compared to age matched healthy controls (Fig. 1(i), Fig. S2(d) in Appendix A). Moreover, α 2,6-sialylation level was increased in sera of *APP/PS1* mice (Fig. S2(e) in Appendix A). The *N*-glycan structures in CSF of AD patients and age matched healthy controls were detected using xCGE-LIF. The PAP of α 2,6-sialylated *N*-glycan in AD patients was significantly higher than those in control group (Fig. S3 in Appendix A). These data reveal that increased α 2,6-sialylation positively correlates with the occurrence of AD.

3.2. ST6Gal-I^{-/-} rats display attenuated Scop-induced AD

ST6Gal-I is an α 2,6-sialyltransferase that catalyzes α 2,6-sialylation (Fig. 2(a)). To further investigate the function of α 2,6-sialylation in AD pathogenesis, we developed an *ST6Gal-I* gene knockout (*ST6Gal-I*^{-/-}) rat model using the CRISPR/Cas9 system (Fig. 2(b)). The offspring genotypes of *ST6Gal-I*^{+/+}, *ST6Gal-I*^{+/-}, and *ST6Gal-I*^{-/-} rats were identified by PCR (Fig. 2(c)). The offspring generated from the intercross of *ST6Gal-I*^{+/-} rats exhibited a basic adherence to Mendelian inheritance (Fig. 2(d)). α 2,6-Sialylation was completely inhibited in the sera of *ST6Gal-I*^{-/-} rats (Fig. 2(e)). There was no significant difference of brain size (Fig. 2(f)), brain wet weight, body, or other crucial organs (liver, kidney, heart, and lung) (Fig. S4 in Appendix A) between male and female *ST6Gal-I*^{+/+} and *ST6Gal-I*^{-/-} rats (at 20 months old). α 2,6-Sialylation was completely inhibited in the brain of *ST6Gal-I*^{-/-} rats, while the other types of glycosylation, including α 2,3-sialylation and fucosylation, were not changed (Fig. 2(g)). As expected, protein expression of ST6Gal-I was absent in brains of *ST6Gal-I*^{-/-} rats, and that of *ST6Gal-I*^{+/-} rats was about 50% of *ST6Gal-I*^{+/+} rats (Fig. 2(h)). Additionally, the mRNA level of *ST6Gal-I* was not detected in brains of *ST6Gal-I*^{-/-} rats compared with *ST6Gal-I*^{+/+} (Fig. 2(i)).

Scop (C17H21NO4) is a tropane alkaloid (Fig. 3(a)). Scop impairs short-term learning and memory in humans and rodents, and induces a variety of cellular changes, including impaired antioxidant defense systems, increased oxidative stress, and neuroinflammation [17]. Scop is an effective pharmacological tool to study the behavioral and molecular changes associated with AD pathogenesis [18]. The Scop-induced AD model was established in *ST6Gal-I*^{-/-} (*ST6Gal-I*^{-/-}-Scop) rats and WT (*ST6Gal-I*^{+/+}-Scop) rats (Fig. 3(a)). We found that deletion of *ST6Gal-I* prevented Scop-mediated reductions in nest-building compared with *ST6Gal-I*^{+/+}-Scop rats (Fig. 3(b)). In the NOR test, *ST6Gal-I*^{-/-}-Scop rats showed high interest in exploring novel objects, as determined by the DI (Fig. 3(c)) and PI (Fig. 3(d)). In the MWM test, escape latency of *ST6Gal-I*^{+/+} rats was increased after Scop-treatment (Fig. S5(a) in Appendix A). Compared with the *ST6Gal-I*^{+/+}-Scop rats the escape latency was decreased in *ST6Gal-I*^{-/-}-Scop rats (Fig. 3(e)), while there is no change of escape latency between *ST6Gal-I*^{+/+} and *ST6Gal-I*^{-/-} rats (Fig. S5(b) in Appendix A). *ST6Gal-I*^{+/+}-Scop rats showed an aimless searching strategy and reduced the time in target quadrant compared to *ST6Gal-I*^{-/-}-Scop rats (Fig. 3(f)). Both *ST6Gal-I*^{+/+}-Scop rats and *ST6Gal-I*^{-/-}-Scop rat groups had similar swimming speed (Fig. 3(g)) and total distance (Fig. 3(h)). These data suggested that ablation of *ST6Gal-I* effectively halts the deterioration of spatial learning and memory capabilities in the rat model treated with Scop.

3.3. Loss of ST6Gal-I reduces BACE1 expression

BACE1 is a key enzyme in A β peptides generation during AD pathogenesis [19]. The BACE1 levels were dramatically increased in Hip of *APP/PS1*-AD mice compared with WT mice (Fig. 4(a)). To investigate α 2,6-sialylation role in BACE1, we compared the expression of BACE1 between *ST6Gal-I*^{+/+} and *ST6Gal-I*^{-/-} brains. Compared to *ST6Gal-I*^{+/+} rats, BACE1 in prefrontal Cor and Hip was down-regulated in *ST6Gal-I*^{-/-} rats (Fig. 4(b)). Immunofluorescence staining showed that BACE1 was also decreased in Hip tissue of *ST6Gal-I*^{-/-} rats (Fig. 4(c)). Moreover, BACE1 enzymatic activity was dramatically reduced in the *ST6Gal-I*^{-/-} brain compared to *ST6Gal-I*^{+/+} brain, as evidenced by ELISA (Fig. 4(d)).

To clarify the association of ST6Gal-I with BACE1 expression, we endeavored to silence the *ST6Gal-I* gene in N2a cells. Initially, we crafted specific *ST6Gal-I* siRNA sequences targeting distinct regions of *ST6Gal-I* open reading frame to assess *ST6Gal-I* knockdown efficacy. The siRNA sequences were aligned with nucleotides 828–848

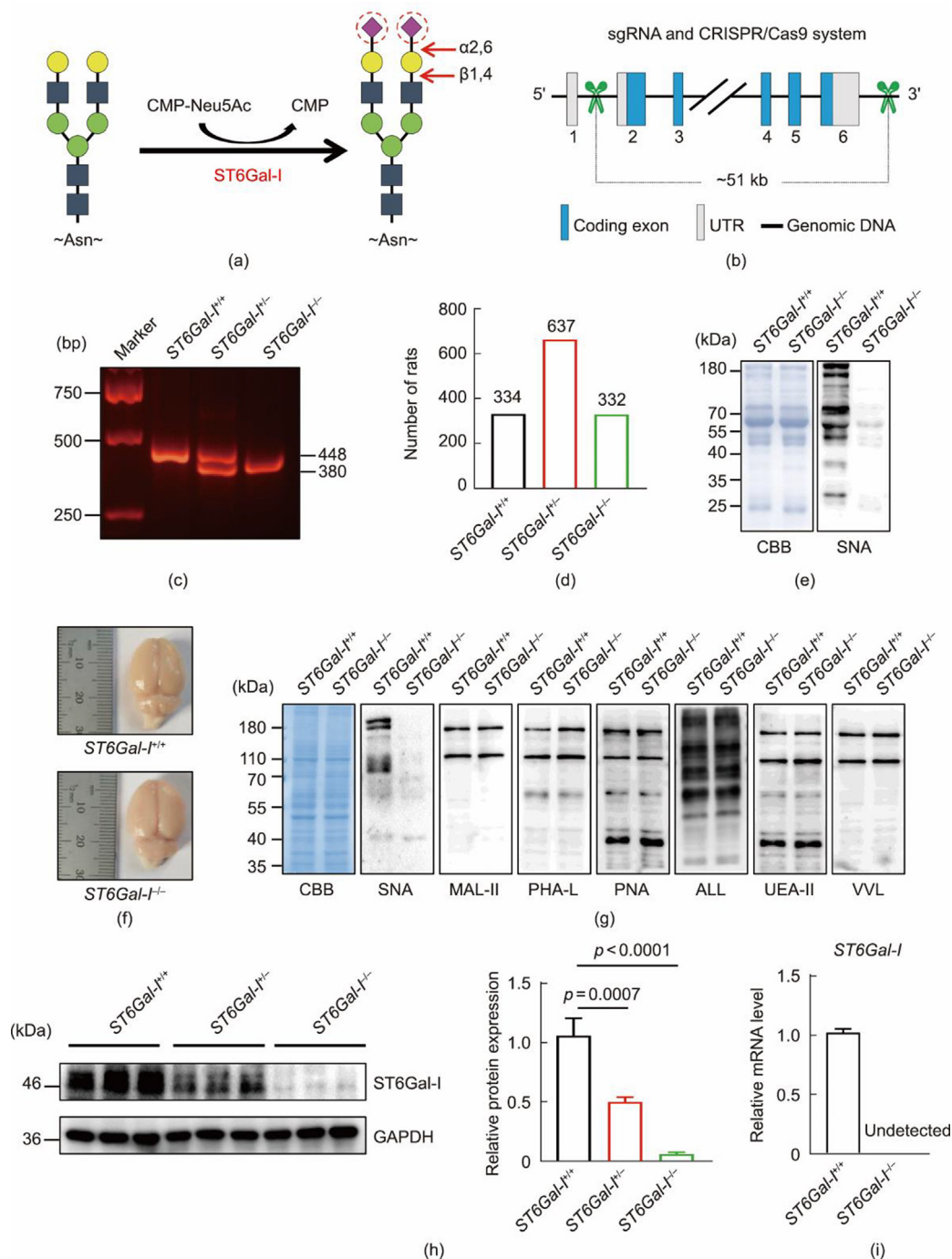


Fig. 2. α2,6-Sialylation was ablated in *ST6Gal-I*^{-/-} rats. (a) Reaction pathway of ST6Gal-I. ST6Gal-I catalyzes the incorporation of α2,6-linked sialic acid, to terminal galactose residues, with cytidine 5'-monophosphate-sialic acid (CMP-Neu5Ac) as the donor. (b) Schematic diagram of CRISPR/Cas9-mediated gene targeting. Small guide RNAs (sgRNAs) targeting exons 2 and 6 of the *ST6Gal-I* gene were micro-injected into the pro-nucleus and about 51 kb DNA was removed. UTR: untranslated regions. (c) Genotyping. The offspring genotypes of *ST6Gal-I*^{+/+}, *ST6Gal-I*^{-/-}, and *ST6Gal-I*^{-/-} rats were validated by PCR. The size of the PCR products was 448 bp (*ST6Gal-I*^{+/+}) and 380 bp (*ST6Gal-I*^{-/-}). (d) Offspring ratio generated from the intercross of *ST6Gal-I*^{-/-} rats was about 1:2:1. (e) SNA blot. α2,6-Sialylation levels in serum samples of *ST6Gal-I*^{+/+} and *ST6Gal-I*^{-/-} rats were detected by SNA lectin (1:10 000), n = 6. (f) After *ST6Gal-I*^{+/+} and *ST6Gal-I*^{-/-} rats (20-month-old) were anesthetized with 10% chloral hydrate, blood in the rats was removed by cardiac perfusion with cooled PBS, and brain tissues were taken for photos, n = 6. (g) Lectin blots. Hip samples (5 μg) of *ST6Gal-I*^{+/+} and *ST6Gal-I*^{-/-} rats were characterized by lectin blotting with SNA, MAL-II, PNA, VVL, AAL, PHA-L, and UEA-II (1:10 000), n = 6. (h) Western blotting (WB). Expression of ST6Gal-I protein in brains of *ST6Gal-I*^{+/+}, *ST6Gal-I*^{-/-}, and *ST6Gal-I*^{-/-} rats (20-month-old) was determined with anti-ST6Gal-I (1:2000) antibody, n = 6. (i) RT-qPCR. The mRNA expression of *ST6Gal-I* in *ST6Gal-I*^{+/+} and *ST6Gal-I*^{-/-} rat brains was detected. The relative expression of *ST6Gal-I* mRNA was normalized to GAPDH, n = 6. Data were presented as the means ± SD. $p < 0.05$ was considered statistically significant.

(siRNA1), 1495–1515 (siRNA2), and 931–951 (siRNA3) of the *ST6Gal-I* gene. Among the three siRNA constructs tested, siRNA1 emerged as the most potent inhibitor of ST6Gal-I expression (Fig. S6 in Appendix A). Next, we designed a pLKO.1 shRNA len-

tivirus system with *ST6Gal-I* siRNA1 and established stable *ST6Gal-I*-KD-N2a cells, and *ST6Gal-I* restored (*ST6Gal-I*-KD-Re) cells. Compared to *ST6Gal-I*-shctl cells, α2,6-sialylation levels were markedly suppressed in the *ST6Gal-I*-KD cells, and re-introduction

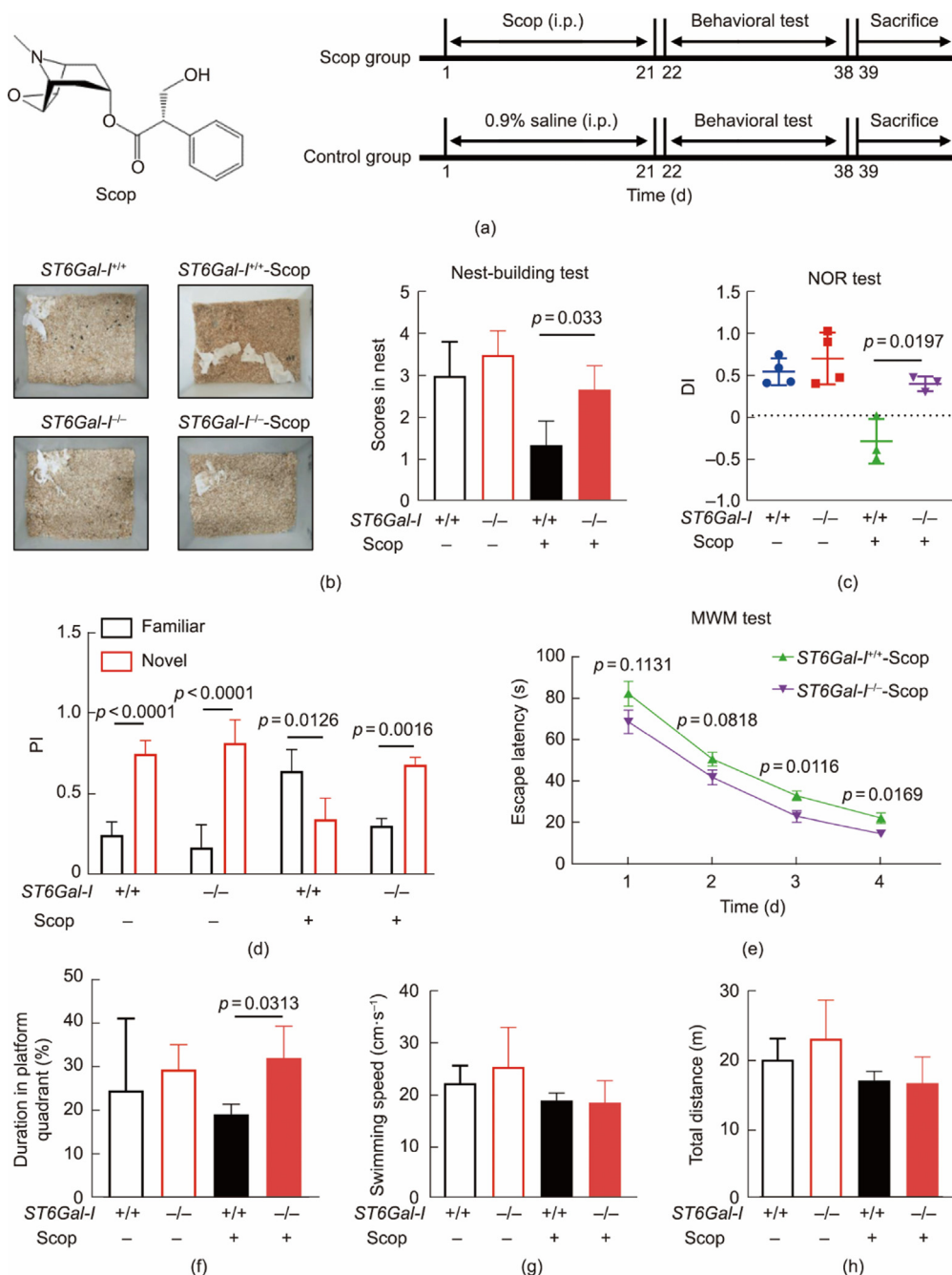


Fig. 3. Ablation of *ST6Gal-I* prevents the loss of spatial learning and memory in the Scop-treated rat model. (a) Schematic of the experimental timeline. *ST6Gal-I*^{-/-} rats and *ST6Gal-I*^{+/+} rats (12-week-old) were given Scop (2 mg·kg⁻¹) or 0.9% saline via intraperitoneal injection every day for 21 d. Rats were then subjected to nest building, NOR, and MWM tests. i.p.: intraperitoneal injection. (b) Representative images from the nest-building experiment with *ST6Gal-I*^{+/+}, *ST6Gal-I*^{-/-}, *ST6Gal-I*^{-/-}-Scop, and *ST6Gal-I*^{+/+}-Scop rats, *n* = 6. Nest-building scores for each group and photos were taken 24 h after the introduction of nesting material to the home cage. (c) DI for each group in the NOR test. (d) PI for each group in the NOR test. (e) Duration of escape within 4 d was analyzed in an MWM experiment. (f) Ratio of time spent in target quadrant for each group. (g) Swimming speed for each group. (h) Total distance for each group. Data were presented as the means ± SD. *p* < 0.05 was considered statistically significant.

of *ST6Gal-I* into *ST6Gal-I*-KD cells resulted in recovery of α2,6-sialylation (Fig. 4(e)). Again, the protein expression of *ST6Gal-I* reflected the degree of α2,6-sialylation (Fig. 4(f)). *ST6Gal-I* mRNA level was reduced in *ST6Gal-I*-KD cells, and restored in the *ST6Gal-I*-KD-Re cells (Fig. 4(g)). *BACE1* expression was dramatically reduced in *ST6Gal-I*-KD cells (Fig. 4(f)), consistent with the findings in the in prefrontal Cor and Hip of *ST6Gal-I*^{-/-} rats (Fig. 4(b)). *BACE1* mRNA expression was also decreased in *ST6Gal-I*-KD cells and recovered in *ST6Gal-I*-KD-Re cells (Fig. 4(h)), suggesting

that *ST6Gal-I* deficiency down-regulated the expression of *BACE1*. As a transcription factor, *SP1* activates the expression of *BACE1*, and participates in the regulation of AD [20,21]. To clarify the role of *SP1* in the mRNA expression of *BACE1*, we predicted the binding relationship between *SP1* and the *BACE1* promoter region through JASPAR website (Fig. S7 in Appendix A). Moreover, the interaction between *SP1* and *BACE1* gene promoter was analyzed by CHIP assay. The binding between *SP1* and *BACE1* gene was suppressed in *ST6Gal-I*-KD cells, and restored in *ST6Gal-I*-KD-Re cells (Fig. 4(i)).

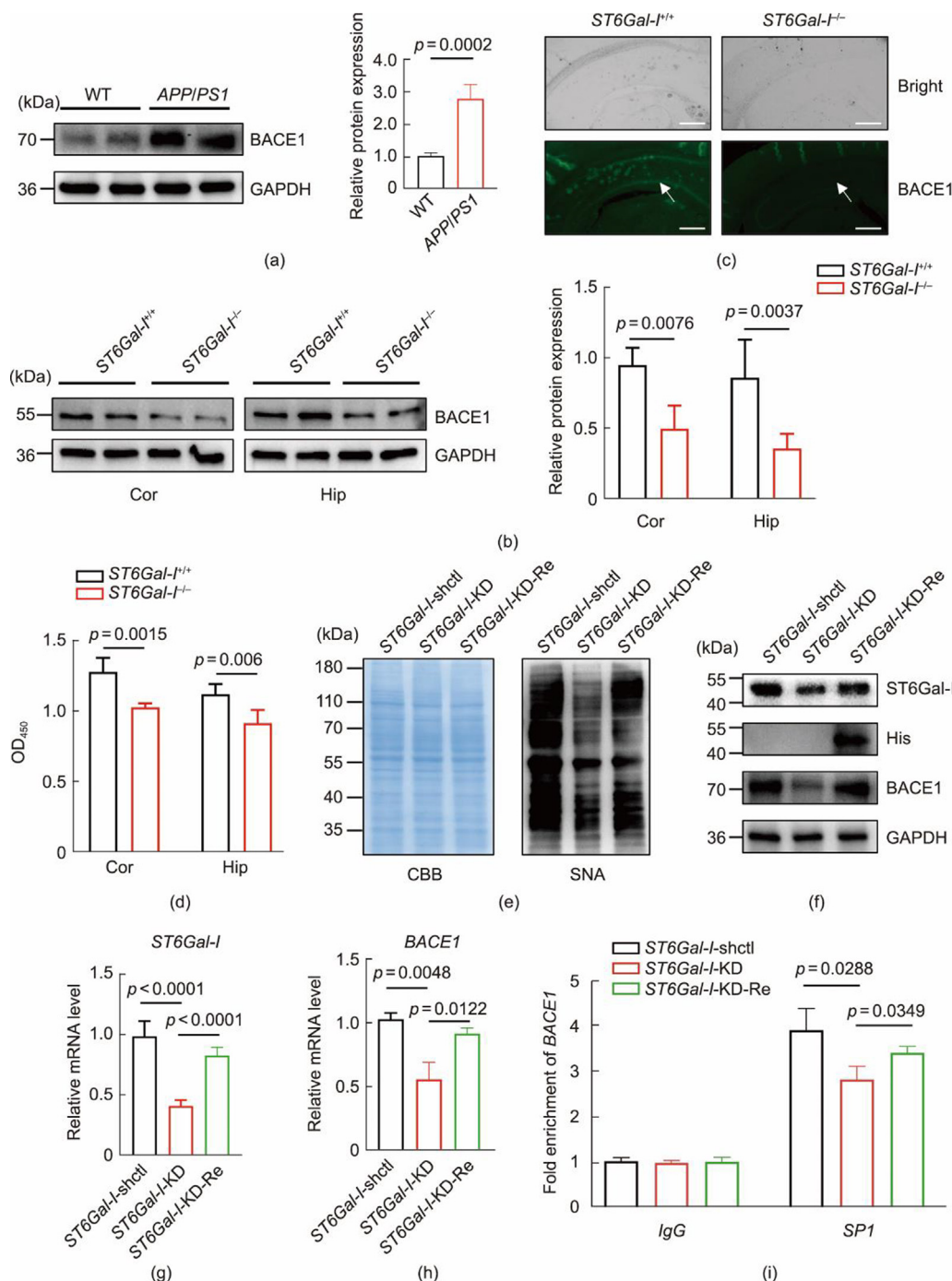


Fig. 4. Loss of *ST6Gal-I* reduces expression of BACE1. (a) BACE1 levels in the Hip of *APP/PS1* mice and age-matched WT mice, $n = 6$. (b) WB shows BACE1 protein levels in the prefrontal Cor and Hip of *ST6Gal-I*^{+/+} and *ST6Gal-I*^{-/-} rats (20-month-old), $n = 6$. (c) Immunofluorescence staining for BACE1 (1:100), *ST6Gal-I*^{+/+} and *ST6Gal-I*^{-/-} rats (20-month-old), $n = 6$, scale bar = 500 μ m. (d) ELISA for BACE1 activity in the prefrontal Cor and Hip of *ST6Gal-I*^{+/+} and *ST6Gal-I*^{-/-} rats, $n = 6$. OD₄₅₀: optical density at 450 nm. (e) α 2,6-Sialylation levels in *ST6Gal-I*-shctl, *ST6Gal-I*-KD, and *ST6Gal-I*-KD-Re cells were determined by SNA (1:10 000) blotting, $n = 3$. (f) Expression of *ST6Gal-I*, His, and BACE1 in *ST6Gal-I*-shctl, *ST6Gal-I*-KD, and *ST6Gal-I*-KD-Re cells was detected by immunoblotting with anti-*ST6Gal-I* (1:2000), anti-His (1:2000), and anti-BACE1 (1:2000), $n = 3$. (g) RT-qPCR assay for the mRNA expression of *ST6Gal-I* in *ST6Gal-I*-shctl, *ST6Gal-I*-KD, and *ST6Gal-I*-KD-Re cells, $n = 6$. The relative expression of *ST6Gal-I* mRNA was normalized to GAPDH. (h) RT-qPCR assay for the mRNA expression of *BACE1* in *ST6Gal-I*-shctl, *ST6Gal-I*-KD, and *ST6Gal-I*-KD-Re cells, $n = 6$. The relative expression of *BACE1* mRNA was normalized to GAPDH. (i) CHIP assay was used to verify the binding of *SP1* to the promoter of the *BACE1* gene in *ST6Gal-I*-shctl, *ST6Gal-I*-KD, and *ST6Gal-I*-KD-Re cells. Data were presented as the means \pm SD. $p < 0.05$ was considered statistically significant.

3.4. Loss of *ST6Gal-I* accelerates degradation of BACE1 via the ubiquitination–proteasome system

N-linked glycosylation occurs in N-X-serine (Ser)/threonine (Thr) sequences, where X can be any amino acid except proline. According to amino acid sequences, we found N-glycosylation

occurs at four conserved asparagine (Asn, N) residues in the N-terminal region of BACE1, namely N¹⁵³, N¹⁷², N²²³, and N³⁵⁴ (Fig. 5(a)). BACE1 was highly α 2,6-sialylated and localized in the Golgi apparatus (Fig. 5(b)). We also found that *ST6Gal-I* interacts with multiple sites of BACE1 in the AlphaFold3 database (Fig. S8 in Appendix A). In order to confirm the N-glycosylation on BACE1,

deglycosylation was performed by peptide-N-glycosidase (PNGase F), which cleaves the amide bond between the first saccharide N-acetylglucosamine (GlcNAc). BACE1 treatment with PNGase F shifted the molecular weight from 70 kDa to approximately 60 kDa. Moreover, the molecular weight of BACE1 was slightly shifted after treatment with neuraminidase 1 (NEU1), which cleaves terminal sialic acids, indicating that BACE1 is a sialylated protein (Fig. 5(c)). IP of BACE1 showed that α 2,6-sialylation of BACE1 was inhibited in *ST6Gal-I*^{-/-} brain (Fig. 5(d)).

To examine whether the degradation of BACE1 protein is governed by ubiquitin–proteasome and/or lysosomes pathways, cells were treated with proteasome inhibitor MG132 or lysosome inhibitor chloroquine (CQ). Degradation of BACE1 was suppressed after MG132 treatment, but not by CQ (Fig. 5(e)), suggesting that degradation of BACE1 is modulated by ubiquitin–proteasome pathway. IP showed that poly-ubiquitination level of BACE1 was increased by knockdown of *ST6Gal-I*, while the expression of BACE1 was reduced (Fig. 5(f)). F-box protein 2 (FBXO2) functions as an E3 ligase that directs BACE1 for ubiquitination and degradation via

F-box domain at early endosome [22]. Loss of *ST6Gal-I* up-regulated FBXO2 expression (Fig. 5(g)). Results indicated that lack of α 2,6-sialylation resulted in increased degradation of BACE1 by the ubiquitination–proteasome system.

3.5. Deletion of *ST6Gal-I* reduces *A β* ₄₂ generation and ameliorates AD pathology

BACE1-mediated APP processing, involving cleavage at the β -site, is the first step leading to A β and sAPP β generation [23]. The content of sAPP β was down-regulated in prefrontal Cor and Hip of *ST6Gal-I*^{-/-} rats, with no significant change in APP expression (Fig. 6(a)), suggesting that the critical role of *ST6Gal-I* in β -cleavage of BACE1. Consistent with results observed in *ST6Gal-I*^{-/-} rats, sAPP β was reduced in *ST6Gal-I*-KD cells, and sAPP β was restored in *ST6Gal-I*-KD-Re (Fig. 6(b)). The levels of APP and sAPP β were dramatically increased in Hip of *APP/PS1*-AD mice compared with WT mice (Fig. 6(c)).

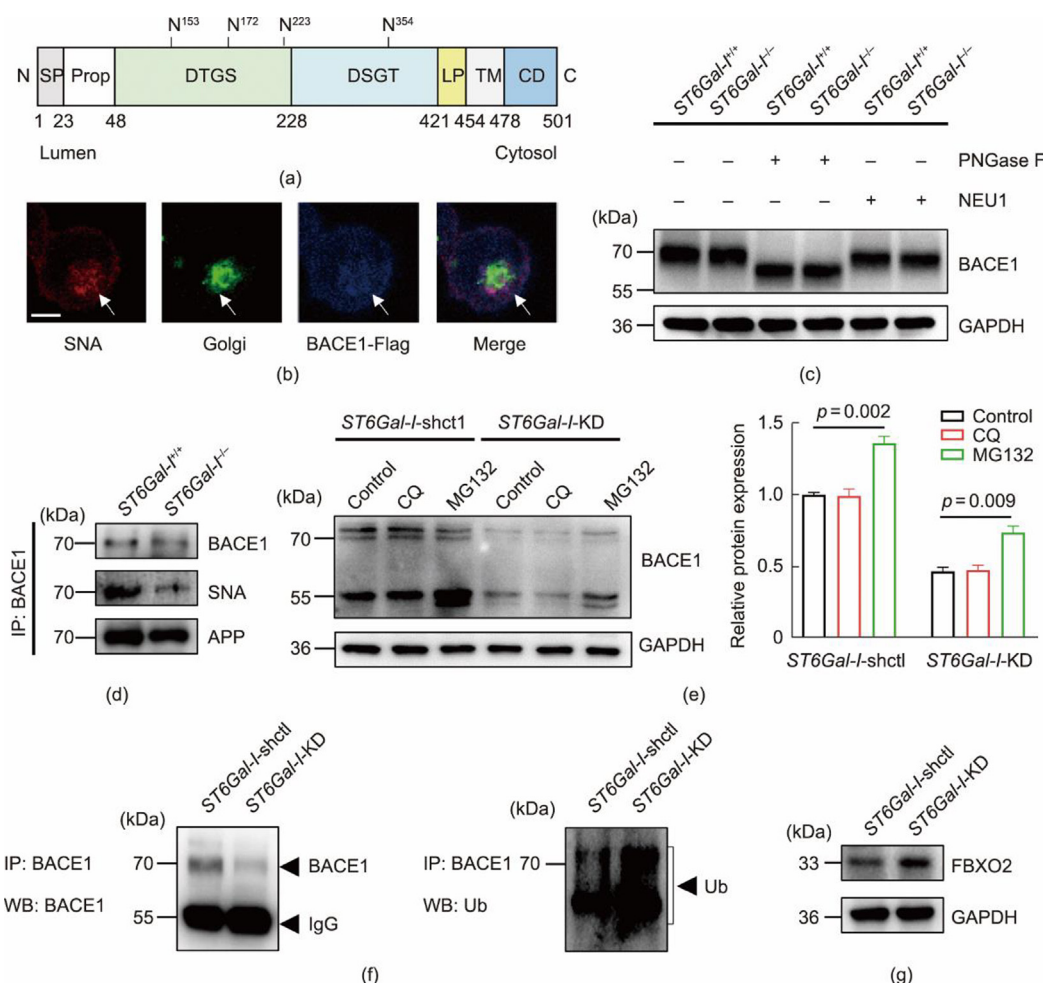


Fig. 5. Loss of *ST6Gal-I* promotes BACE1 ubiquitination (Ub) and proteasomal degradation. (a) BACE1 structure showing the various subdomains of BACE1. The two signature aspartic acid protease active site motifs at position 93 (DTGS) and position 289 (DSGT) are marked. Numbers refer to amino acid positions. N¹⁵³, N¹⁷², N²²³, and N³⁵⁴ represent positions of N-linked glycosylation. CD: cytosolic domain; LP: loop; Prop: pro-peptide; SP: signal peptide; TM: transmembrane region. (b) Co-localization of *ST6Gal-I* and BACE1 in N2a cells. Cells were stained with SNA (1:100, red), anti-Golgi apparatus (1:50, green), and anti-BACE1 (1:100, blue) antibodies and then subjected to confocal fluorescence microscopy, scale bar = 10 μ m. (c) Sialylation of BACE1. *ST6Gal-I*^{+/+} and *ST6Gal-I*^{-/-} brains (3-month-old) were lysed and then treated with or without PNGase F (300 ng) or NEU1 (500 ng) for 24 h. The location of BACE1 from *ST6Gal-I*^{+/+} and *ST6Gal-I*^{-/-} brains were detected by WB, n = 6. (d) IP of BACE1. Proteins from *ST6Gal-I*^{+/+} and *ST6Gal-I*^{-/-} brains were immunoprecipitated, immunoblotted, and probed with anti-BACE1 (1:2000), SNA (1:2000), anti-APP (1:2000) antibodies, n = 6. (e) WB. The *ST6Gal-I*-shct1 and *ST6Gal-I*-KD cells were treated with or without CQ (25 μ mol·L⁻¹) or MG132 (40 μ mol·L⁻¹) for 4 h, then subjected to WB with anti-BACE1 (1:2000) antibodies. (f) BACE1 ubiquitination. BACE1 protein was immunoprecipitated from *ST6Gal-I*-shct1 and *ST6Gal-I*-KD cells and immunoblotted with anti-BACE1 (1:2000) or anti-Ub antibodies (1:2000), n = 3. (g) Expression of FBXO2. WB was used to analyze the FBXO2 level of *ST6Gal-I*-shct1 and *ST6Gal-I*-KD cells. Data were presented as the means \pm SD. p < 0.05 was considered statistically significant.

To explore the ability of BACE1 to cleave APP, we generated BACE1-OE N2a cells with markedly increased BACE1 mRNA and protein (Fig. 6(d)). Flag-labeled BACE1 was purified from BACE1-

OE N2a cells and de-sialylated BACE1 was obtained by treatment with NEU1 (Fig. 6(e)). The levels of A β ₄₂ were dramatically reduced following incubation with de-sialylated BACE1, when the APP and

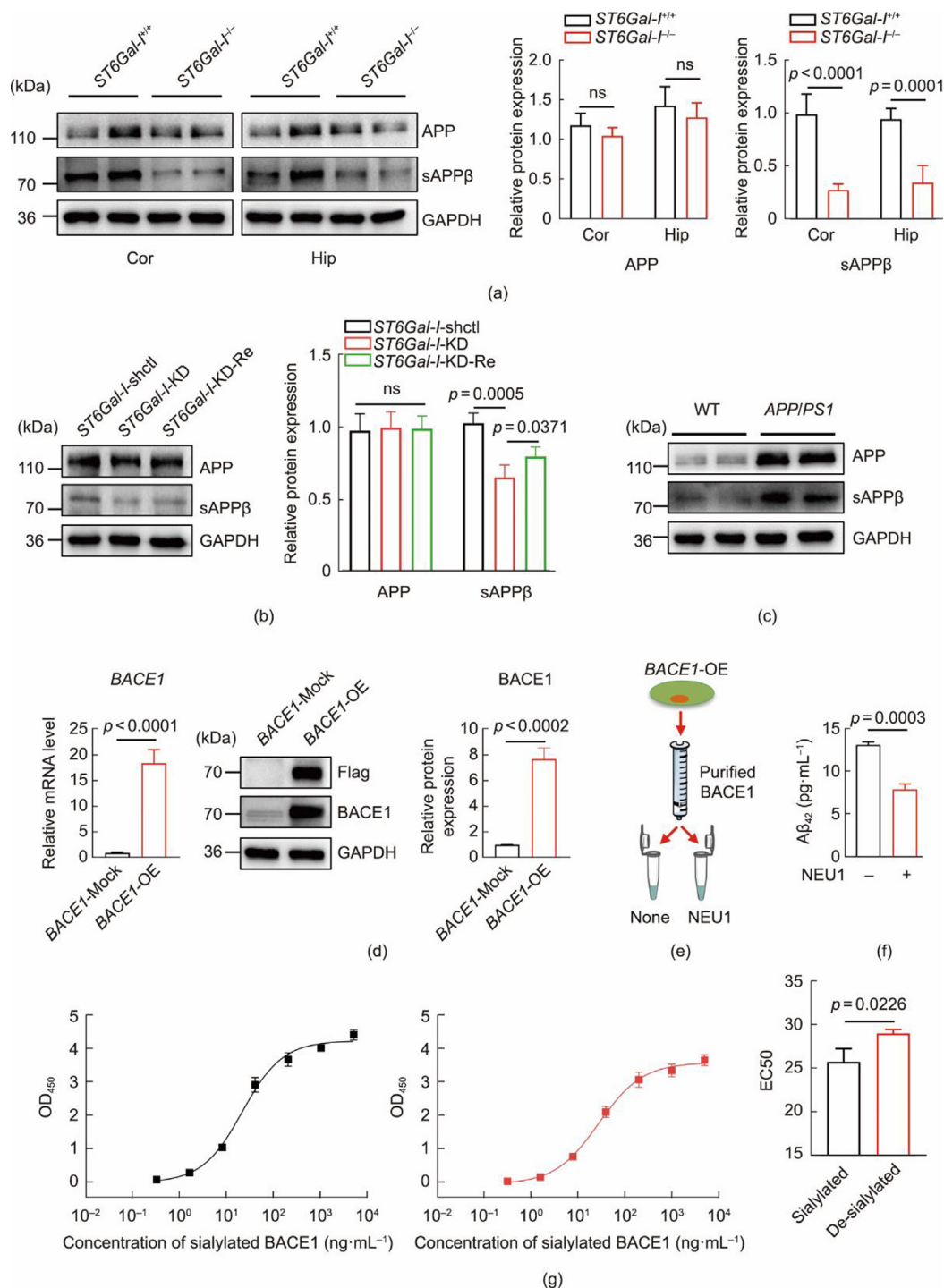


Fig. 6. Ablation of *ST6Gal-I* reduces β -cleavage. (a) Expression of APP and sAPP β in the prefrontal Cor and Hip. The prefrontal Cor and Hip of *ST6Gal-I*^{+/+} ($n = 6$) and *ST6Gal-I*^{-/-} ($n = 6$) brains were lysed and the expression of APP and sAPP β was determined by WB with anti-APP (1:2000) and anti-sAPP β (1:500) antibodies. (b) WB. APP and sAPP β protein levels in *ST6Gal-I*-shctl, *ST6Gal-I*-KD and *ST6Gal-I*-KD-Re cells were determined by WB with anti-APP (1:2000) and anti-sAPP β (1:500) antibodies. (c) WB was used to compare APP and sAPP β levels in the Hip of *APP/PS1* mice ($n = 6$) and age-matched WT mice ($n = 4$) following probing with anti-APP (1:2000) and anti-sAPP β (1:500) antibodies. (d) Establishment of *BACE1*-OE N2a cells. Expression of BACE1 and Flag in *BACE1*-Mock and *BACE1*-OE N2a cells were detected by immunoblotting and probing with anti-BACE1 (1:2000) and anti-Flag (1:2000), $n = 3$. The mRNA expression of *BACE1* in *BACE1*-Mock ($n = 6$) and *BACE1*-OE N2a ($n = 6$) cells were determined. The relative expression of *BACE1* mRNA was normalized to GAPDH. (e) *BACE1*-Flag proteins were purified from *BACE1*-OE N2a cells according to the manufacturer's protocol Anti-Flag Affinity gel kit. *BACE1*-Flag proteins were divided into two portions, one *BACE1*-Flag protein was incubated NEU1 (100 ng) for 24 h and the other one was not treated. (f) A β ₄₂ production by BACE1. A β ₄₂ level in the protein lysates treated with or without NEU1 (100 ng) were measured by a sandwich ELISA kit, $n = 6$. (g) APP-BACE1 interaction. Fitting curve of a series of concentrations, 0.32, 1.6, 8, 40, 200, 1000, 5000 ng mL⁻¹ of sialylated or de-sialylated BACE1 incubated with APP, $n = 3$. Data were presented as the means \pm SD. $p < 0.05$ was considered statistically significant.

BACE1 were incubated for at 4 °C for 24 h with gentle shaking, indicating that de-sialylation reduced the efficiency of BACE1 to cleave APP (Fig. 6(f)). In the IP assay, loss of α 2,6-sialylation also reduced the affinity of BACE1 to cleave APP (Fig. 5(d)). To further investigate whether α 2,6-sialylation affects the affinity of BACE1 and APP, we added intact BACE1 and de-sialylated BACE1 to the reaction buffer. The median effect concentration (EC50) value for the interaction between de-sialylated BACE1 and APP demonstrated about 30% augmentation, indicating that loss of α 2,6-sialylation suppressed the interaction between BACE1 and APP (Fig. 6(g)).

The level of A β ₄₂ is increased in Hip of APP/PS1-AD mice (Fig. 7(a)) [24]. To further determine the role of ST6Gal-I on A β ₄₂ generation, we measured A β ₄₂ levels in ST6Gal-I-KD cells by a sandwich ELISA kit. Production of A β ₄₂ was reduced in culture media and lysates of ST6Gal-I-KD cells, and restored by re-introduction of ST6Gal-I (Fig. 7(b)). Various A β peptide deposits have been shown to induce mitochondria-mediated extrinsic and intrinsic apoptosis in cerebral endothelial cells, and aggravate AD pathology [25]. Knockdown of ST6Gal-I suppressed the expression of caspase-3, cleaved caspase-3, cleaved caspase-9, P53, and Bad, which are pro-apoptotic factors. Conversely, anti-apoptotic protein Bcl-2 was increased in ST6Gal-I-KD cells (Fig. 7(c)).

Subsequently, we compared the transcriptome between ST6Gal-I-KD and ST6Gal-I-shctl cells. Compared to ST6Gal-I-shctl, ST6Gal-I-KD had a total of 1058 up-regulated genes and 1348 down-regulated genes (Fig. 7(d)). In addition, the Gene Ontology analysis showed that genes might participate in “regulation of neurogenesis,” “learning or memory,” “connective tissue development,” “neuron projection guidance,” and “neuron to neuron synapse” (Fig. S9 in Appendix A). Furthermore, the Kyoto Encyclopedia of Genes and Genomes (KEGG) pathway showed that genes involved in “Wnt signaling pathway” and “transforming growth factor- β (TGF- β) signaling pathway” in ST6Gal-I-KD were increased, while “apoptosis” and “mitogen-activated protein kinase (MAPK) signaling pathway” were decreased (Fig. 7(e)), suggesting that ST6Gal-I plays multiple roles in reducing A β production, alleviating cognitive impairment and reducing apoptosis.

4. Discussion

Although glycosylation is modified by a variety of glycosyltransferases, it is a highly ordered process with each glycosyltransferase. The glycosylation modification may be determined by a paracentral dogma acting in parallel with the existing central dogma [26]. Several studies have reported the correlation of abnormal glycosylation with the occurrence of AD. The bisecting GlcNAc modification by GnT-III is increased in AD patient brains [27], and reduced O-GlcNAcylation is associated with development of AD [28]. The levels of α -mannosides and α -glucosides are reduced in sera of AD patients [29]. Moreover, the rs3936289 single-nucleotide polymorphism (SNP) in ST6Gal-I is closely related to the conversion from MCI to AD [30]. However, the relationship between α 2,6-sialylation by ST6Gal-I and AD occurrence is poorly understood. In the present study, we first found the hyper α 2,6-sialylation catalyzed by ST6Gal-I in the AD patients and APP/PS1-AD model mice. Then, we used ST6Gal-I^{-/-} rat model to clarify the correlation between ST6Gal-I and AD occurrence. ST6Gal-I increases BACE1 expression, which, in turn, leads to A β ₄₂ deposition in AD. Loss of ST6Gal-I accelerates degradation of BACE1 specially, and BACE1 plays a crucial role as key enzyme in A β peptides biosynthesis during AD pathogenesis. The MWM, NOR, and nest-building tests showed that ST6Gal-I^{-/-} rats alleviated the cognitive impairment of AD by reduced BACE1 expression (Fig. 8).

BACE1 undergoes post-translational modifications during maturation, including glycosylation and ubiquitination. BACE1 is mod-

ified by N-glycosylation at N¹⁵³, N¹⁷², N²²³, and N³⁵⁴ in lumen of ER, and change of N-glycosylation site of BACE1 decreased its proteolytic activity [31,32]. Kizuka et al. [27] have reported that BACE1 is modified with bisecting GlcNAc, and absence of bisecting GlcNAc modifications results in the translocation of BACE1. We first found that BACE1 is a hyper-sialylated protein and co-localizes predominantly with α 2,6-sialylation in the Golgi apparatus. Mature BACE1 is transported to cell membrane surface or Golgi apparatus and then degraded by endosome-lysosome and/or by ubiquitin-proteasome pathway [33,34]. Kang et al. [35] found that the ubiquitination at Lys⁵⁰¹ or at Lys⁶³ regulates Golgi-localized γ -ear-containing ADP ribosylation factor 1 (ARF)-binding protein (GGA3)-mediated degradation of BACE1. Wang et al. [36] also reported that ubiquitination at Lys²⁰³ and Lys³⁸² are crucial for proteasomal degradation of BACE1. The present study shows deletion of ST6Gal-I downregulates the expression of BACE1 via ubiquitin-proteasome pathway by accelerating its ubiquitination. The reduced BACE1 was restored by MG132 treatment, suggesting that de-sialylated BACE1 undergoes fast protein degradation. Several mechanisms may contribute to the reduced BACE1 expression by ST6Gal-I ablation. First, deletion of ST6Gal-I enhances the expression of FBXO2. As an E3-ligase of BACE1, FBXO2 increases BACE1 ubiquitination and its subsequent proteasomal degradation [22]. Second, α 2,6-sialylation on BACE1 N-glycans influences its ubiquitination directly. Because N²²³ and N³⁵⁴ are near the ubiquitination sites (Lys²⁰³, Lys³⁸², Lys⁵⁰¹, Lys⁶³) of BACE1, α 2,6-sialylation can mediate the steric and hydrophilic interactions between the N-glycan and the neighboring ubiquitination site. Third, α 2,6-sialylation may alter the conformational preferences of BACE1 and influence BACE1 enzymatic activity. Loss of bisecting GlcNAc on BACE1 suppresses its enzymatic activity [27,37]. Therefore, we have sufficient reason to believe that lacking α 2,6-sialylation on BACE1 may affect its expression and enzymatic activity. Intriguingly, ST6Gal-I serves as one of the physiological substrates for BACE1. BACE1 cleave between Lys⁴⁰ and Glu⁴¹ of ST6Gal-I, and produce soluble ST6Gal-I [38]. The expression of ST6Gal-I was also increased in plasma of BACE1-transgenic mice [39].

Abnormal N-glycosylation is involved with the production of A β ₄₂ peptides. For example, the deficiency in GnT-III diminishes A β -plaque formation in the brain by enhancing the lysosomal degradation of BACE1 [27]. Increased O-GlcNAcylation protects against τ and A β peptide toxicity [28]. In our study, A β ₄₂ levels were reduced in ST6Gal-I-KD and ST6Gal-I-KD-Re cells, indicating that ST6Gal-I can regulate A β ₄₂ production. It is interesting that deposition of A β protein triggers the apoptotic pathway, leading to neuronal death, therefore, apoptosis is thought to be the cause of AD-related manifestations [40]. The expression of several pro-apoptotic proteins is decreased in ST6Gal-I-KD cells, while the expression of anti-apoptotic proteins is increased. Furthermore, deletion of ST6Gal-I alleviates the impairment of learning and memory caused by Scop in nest building, WMW, and NOR tests.

Given that sialylation is an important post-translational process and modulates the functions of multiple proteins, the observation that sialylation regulates AD generation is perhaps not surprising. Transcriptome analysis showed that knockdown of ST6Gal-I gene increases the Wnt and TGF- β signaling pathways and reduces MAPK signaling pathways. The Wnt signaling pathway exacerbates to AD pathogenesis through the elicitation of synaptic impairment, neuronal deterioration, and increased neuronal vulnerability to A β -mediated apoptosis [41,42]. However, neuronal TGF- β 1 signaling promotes the A β clearance and reduces the neurodegeneration in AD [43,44]. On the contrary, ST6Gal-I inhibition could reduce the MAPK signaling pathways. Inhibition of the MAPK pathway can suppress apoptosis of hippocampal neurons [44]. It has been reported that inhibition of the MAPK signal pathway reduces A β

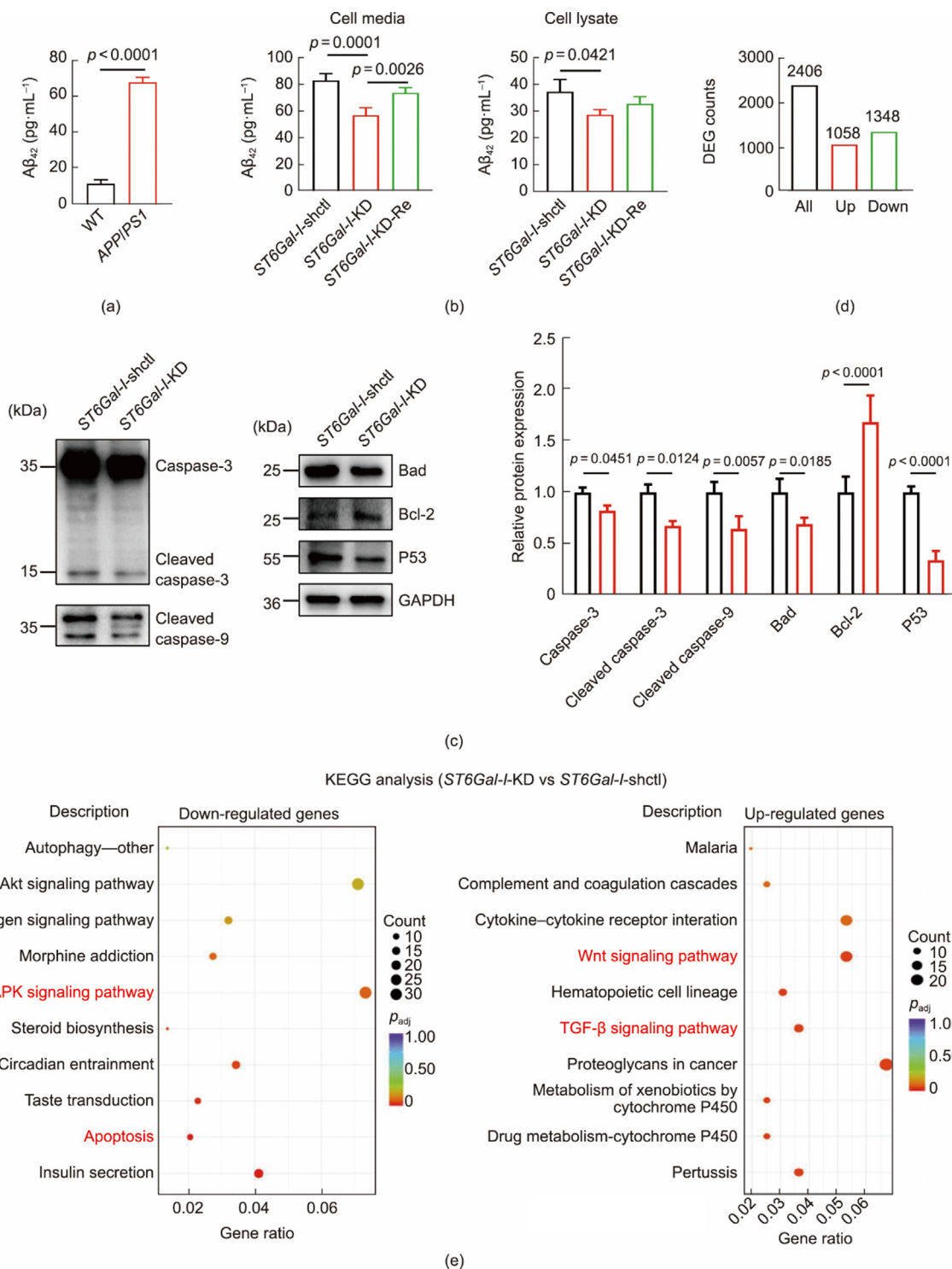


Fig. 7. Ablation of *ST6Gal-I* reduces $A\beta_{42}$ generation. (a) $A\beta_{42}$ level in the Hip of *APP/PS1* mice and age-matched WT mice was measured using a sandwich ELISA kit, $n = 6$. (b) Comparison of the $A\beta_{42}$ relative level in *ST6Gal-I-shctl*, *ST6Gal-I-KD*, and *ST6Gal-I-KD-Re* cells by a sandwich ELISA kit, $n = 6$. (c) Expression of apoptosis-related proteins. *ST6Gal-I-shctl* and *ST6Gal-I-KD* cells were lysed and the expression levels of Bad (1:1000), Bcl-2 (1:1000), caspase-3, cleaved caspase-3 (1:1000), cleaved caspase-9 (1:2000), and P53 (1:1000) proteins were analyzed by WB, $n = 3$. (d) Histogram of differentially-expressed genes in *ST6Gal-I-KD* cells compared to *ST6Gal-I-shctl* cells. (e) KEGG enrichment analysis of differentially-expressed genes in *ST6Gal-I-KD* cells compared to *ST6Gal-I-shctl* cells. PI3K: phosphoinositide 3-kinase; Akt: protein kinase B; p_{adj} : adjusted p value. Data were presented as the means \pm SD. $p < 0.05$ was considered statistically significant.

generation and alleviates cognitive impairments in *APP/PS1*-AD model mice [45].

In summary, we initial findings revealed a significant association between α 2,6-sialylation and the onset as well as the progression of AD. Knockout/knockdown of *ST6Gal-I* reduces the

expression of BACE1 through the ubiquitin–proteasome pathway and alleviates $A\beta_{42}$ -induced apoptosis to inhibit AD progression. As the key rate-limiting enzyme in the production of $A\beta$, BACE1 stands out as a prime therapeutic target for reducing brain $A\beta$ levels in AD [46]. The suppression of BACE1 production or the

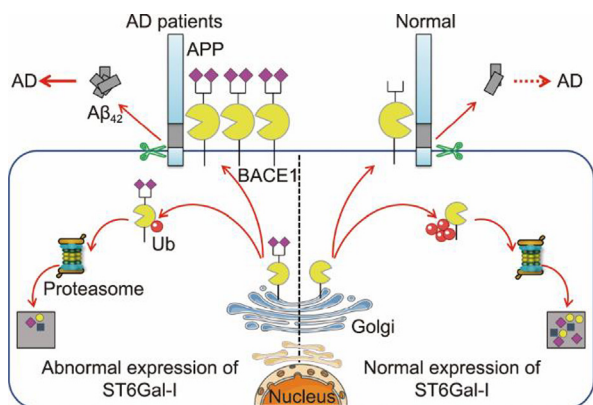


Fig. 8. Model for the dysregulation of BACE1 and α 2,6-sialylation in AD. In AD patients, we propose the existence of highly expressed α 2,6-sialylation catalyzed by ST6Gal-I. This ST6Gal-I-mediated α 2,6-sialylation of BACE1 regulates BACE1 expression by affecting BACE1 ubiquitination (Ub) levels. Increased α 2,6-sialylation on BACE1 enhances $A\beta_{42}$ deposition, which is a feature of AD patients.

enhancement of BACE1 degradation has proven to be a beneficial disease-modifying therapeutic strategy to combat the cell death and cognitive impairments associated with this challenging neurodegenerative disorder. Our study has important biological implications for the diagnosis and treatment of AD from glyco-biological aspects.

CRediT authorship contribution statement

Kangkang Yang: Writing – original draft, Visualization, Validation, Software, Formal analysis. **Xueying Li:** Supervision, Software, Methodology, Investigation, Formal analysis, Data curation. **Minchao Lai:** Writing – original draft, Resources, Project administration, Conceptualization. **Weimei Zhao:** Supervision, Software, Data curation, Conceptualization. **Wanli Song:** Visualization, Software, Resources, Conceptualization. **Shaobin Chen:** Project administration, Methodology. **Wenzhe Li:** Writing – review & editing, Project administration, Investigation, Funding acquisition, Conceptualization.

Declaration of competing interest

The authors declare that they have no known competing financial interests or personal relationships that could have appeared to influence the work reported in this paper.

Acknowledgments

This work was supported by grants from the National Natural Science Foundation of China (32171279), the Guangdong Basic and Applied Basic Research Foundation (2024A1515012796), the Scientific Research Initiation Grant from Shantou University Medical College (510858066), and the Provincial Science and Technology Innovation Strategy Special City and County Science and Technology Innovation Support Project (STKJ2023008).

Appendix A. Supplementary data

Supplementary data to this article can be found online at <https://doi.org/10.1016/j.eng.2025.02.016>.

References

- [1] Jia J, Ning Y, Chen M, Wang S, Yang H, Li F, et al. Biomarker changes during 20 years preceding Alzheimer's disease. *N Engl J Med* 2024;390(8):712–22.
- [2] Ashrafian H, Zadeh EH, Khan RH. Review on Alzheimer's disease: inhibition of amyloid β and τ tangle formation. *Int J Biol Macromol* 2021;167:382–94.
- [3] Capitini C, Bigi A, Parenti N, Emanuele M, Bianchi N, Cascella R, et al. APP and BACE1: differential effect of cholesterol enrichment on processing and plasma membrane mobility. *iScience* 2023;26(5):106611.
- [4] Xu Y, Jiang H, Zhu B, Cao M, Feng T, Sun Z, et al. Advances and applications of fluids biomarkers in diagnosis and therapeutic targets of Alzheimer's disease. *CNS Neurosci Ther* 2023;29(8):2060–73.
- [5] Cheng X, He P, Lee T, Yao H, Li R, Shen Y. High activities of BACE1 in brains with mild cognitive impairment. *Am J Pathol* 2014;184(1):141–7.
- [6] Willem M, Dewachter I, Smyth N, Van Dooren T, Borghgraef P, Haass C, et al. β -Site amyloid precursor protein cleaving enzyme 1 increases amyloid deposition in brain parenchyma but reduces cerebrovascular amyloid angiopathy in aging BACE \times APP[V717I] double-transgenic mice. *Am J Pathol* 2004;165(5):1621–31.
- [7] Ohno M, Cole S, Yasvoina M, Zhao J, Citron M, Berry R, et al. BACE1 gene deletion prevents neuron loss and memory deficits in 5XFAD APP/PS1 transgenic mice. *Neurobiol Dis* 2007;26(1):134–45.
- [8] Kizuka Y, Kitazume S, Taniguchi NJ. N-glycan and Alzheimer's disease. *Biochim Biophys Acta Gen Subj* 2017;1861(10):2447–54.
- [9] Shibuya N, Goldstein I, Broekaert W, Nsimba-Lubaki M, Peeters B, Peumans WJ. The elderberry (*Sambucus nigra* L.) bark lectin recognizes the Neu5Ac(α 2-6)Gal/GalNAc sequence. *J Biol Chem* 1987;262(4):1596–601.
- [10] Lin Y, Lubman DM. The role of N-glycosylation in cancer. *Acta Pharm Sin B* 2024;14(3):1098–110.
- [11] Yang K, Yang Z, Chen X, Li W. The significance of sialylation on the pathogenesis of Alzheimer's disease. *Brain Res Bull* 2021;173:116–23.
- [12] Morris R. Developments of a water-maze procedure for studying spatial learning in the rat. *J Neurosci Methods* 1984;11(1):47–60.
- [13] Zhou Y, Zhu F, Liu Y, Zheng M, Wang Y, Zhang D, et al. Blood-brain barrier-penetrating siRNA nanomedicine for Alzheimer's disease therapy. *Sci Adv* 2020;6(41):eabc7031.
- [14] Lueptow LM. Novel object recognition test for the investigation of learning and memory in mice. *J Vis Exp* 2017;126:55718.
- [15] Hennig R, Cajic S, Borowiak M, Hoffmann M, Kottler R, Reichl U, et al. Towards personalized diagnostics via longitudinal study of the human plasma N-glycome. *Biochim Biophys Acta* 2016;1860(8):1728–38.
- [16] Liu XQ, Hu T, Wu GL, Qiao LJ, Cai YF, Wang Q, et al. Tanshinone IIA, the key compound in *Salvia miltiorrhiza*, improves cognitive impairment by upregulating $A\beta$ -degrading enzymes in APP/PS1 mice. *Int J Biol Macromol* 2024;254(Pt 2):127923.
- [17] Tang KS. The cellular and molecular processes associated with scopolamine-induced memory deficit: a model of Alzheimer's biomarkers. *Life Sci* 2019;233:116695.
- [18] Hernández-Rodríguez M, Arciniega-Martínez I, García-Marín I, Correa-Basurto J, Rosales-Hernández MJM. Chronic administration of scopolamine increased GSK3 β , p9, β secretase, amyloid β , and oxidative stress in the hippocampus of Wistar rats. *Mol Neurobiol* 2020;57(9):3979–88.
- [19] Singh AK, Pati U. CHIP stabilizes amyloid precursor protein via proteasomal degradation and p53-mediated trans-repression of β -secretase. *Ageing Cell* 2015;14(4):595–604.
- [20] Nong W, Bao C, Chen Y, Wei Z. miR-212-3p attenuates neuroinflammation of rats with Alzheimer's disease via regulating the SP1/BACE1/NLRP3/caspase-1 signaling pathway. *Bosn J Basic Med Sci* 2022;22(4):540–52.
- [21] Wei C, Zhang W, Zhou Q, Zhao C, Du Y, Yan Q, et al. Mithramycin A alleviates cognitive deficits and reduces neuropathology in a transgenic mouse model of Alzheimer's disease. *Neurochem Res* 2016;41(8):1924–38.
- [22] Gong B, Chen F, Pan Y, Arrieta-Cruz I, Yoshida Y, Haroutunian V, et al. SCF^{Fbx2}-E3-ligase-mediated degradation of BACE1 attenuates Alzheimer's disease amyloidosis and improves synaptic function. *Ageing Cell* 2010;9(6):1018–31.
- [23] Zimmer VC, Lauer AA, Hauptenthal V, Stahlmann CP, Mett J, Grösgen S, et al. A bidirectional link between sulfatide and Alzheimer's disease. *Cell Chem Biol* 2024;31(2):265–83.e7.
- [24] Zhang M, Wang W, Ye Q, Fu Y, Li X, Yang K, et al. Histone deacetylase inhibitors VPA and WT161 ameliorate the pathological features and cognitive impairments of the APP/PS1 Alzheimer's disease mouse model by regulating the expression of APP secretases. *Alzheimers Res Ther* 2024;16(1):15.
- [25] Wong K, Roy J, Fung M, Heng B, Zhang C, Lim LJA, et al. Relationships between mitochondrial dysfunction and neurotransmission failure in Alzheimer's disease. *Ageing Dis* 2020;11(5):1291–316.
- [26] Wang W. Glycomedicine: the current state of the art. *Engineering* 2023;26:12–5.
- [27] Kizuka Y, Kitazume S, Fujinawa R, Saito T, Iwata N, Saido T, et al. An aberrant sugar modification of BACE1 blocks its lysosomal targeting in Alzheimer's disease. *EMBO Mol Med* 2015;7(2):175–89.
- [28] Pinho T, Verde D, Correia S, Cardoso S, Moreira P. O-GlcNAcylation and neuronal energy status: implications for Alzheimer's disease. *Ageing Res Rev* 2018;46:32–41.
- [29] Sun X, Ma R, Yao X, Shang X, Wang Q, Wang J, et al. Concanavalin agglutinin levels are decreased in peripheral blood of Alzheimer's disease patients. *J Alzheimer's Dis* 2016;49(1):63–72.
- [30] Lee E, Giovanello K, Saykin A, Xie F, Kong D, Wang Y, et al. Single-nucleotide polymorphisms are associated with cognitive decline at Alzheimer's disease conversion within mild cognitive impairment patients. *Alz Dement-Dadm* 2017;8:86–95.
- [31] Regan P, McClean P, Smyth T, Doherty MJM. Early stage glycosylation biomarkers in Alzheimer's disease. *Medicines* 2019;6(3):92.

- [32] Charlwood J, Dingwall C, Matico R, Hussain I, Johanson K, Moore S, et al. Characterization of the glycosylation profiles of Alzheimer's β -secretase protein Asp-2 expressed in a variety of cell lines. *J Biol Chem* 2001;276(20):16739–48.
- [33] Koh Y, von Arnim C, Hyman B, Tanzi R, Tesco G. BACE is degraded via the lysosomal pathway. *J Biol Chem* 2005;280(37):32499–504.
- [34] Qing H, Zhou W, Christensen M, Sun X, Tong Y, Song W. Degradation of BACE by the ubiquitin–proteasome pathway. *FASEB J* 2004;18(13):1571–3.
- [35] Kang E, Cameron A, Piazza F, Walker K, Tesco G. Ubiquitin regulates GGA3-mediated degradation of BACE1. *J Biol Chem* 2010;285(31):24108–19.
- [36] Wang R, Ying Z, Zhao J, Zhang Y, Wang R, Lu H, et al. Lys203 and Lys382 are essential for the proteasomal degradation of BACE1. *Curr Alzheimer Res* 2012;9(5):606–15.
- [37] Wen W, Li P, Liu P, Xu S, Wang F, Huang J. Post-translational modifications of BACE1 in Alzheimer's disease. *Curr Neuropharmacol* 2022;20(1):21122.
- [38] Kitazume S, Tachida Y, Oka R, Shirota K, Saido T, Hashimoto Y. Alzheimer's β -secretase, β -site amyloid precursor protein-cleaving enzyme, is responsible for cleavage secretion of a Golgi-resident sialyltransferase. *PNAS* 2001;98(24):13554–9.
- [39] Kitazume S, Nakagawa K, Oka R, Tachida Y, Ogawa K, Luo Y, et al. *In vivo* cleavage of α 2,6-sialyltransferase by Alzheimer β -secretase. *J Biol Chem* 2005;280(9):8589–95.
- [40] Kumari S, Dhapola R, Reddy DH. Apoptosis in Alzheimer's disease: insight into the signaling pathways and therapeutic avenues. *Apoptosis* 2023;28(7–8):943–57.
- [41] Martínez M, Inestrosa NC. The transcriptional landscape of Alzheimer's disease and its association with Wnt signaling pathway. *Neurosci Biobehav Rev* 2021;128:454–66.
- [42] Zhang Z, Hartmann H, Do V, Abramowski D, Sturchler-Pierrat C, Staufenbiel M, et al. Destabilization of β -catenin by mutations in presenilin-1 potentiates neuronal apoptosis. *Nature* 1998;395(6703):698–702.
- [43] Hu Y, Chen W, Wu L, Jiang L, Liang N, Tan L, et al. TGF- β 1 restores hippocampal synaptic plasticity and memory in Alzheimer model via the PI3K/Akt/Wnt/ β -catenin signaling pathway. *J Mol Neurosci* 2019;67(1):142–9.
- [44] Samuels I, Karlo J, Faruzzi A, Pickering K, Herrup K, Sweatt J, et al. Deletion of *ERK2* mitogen-activated protein kinase identifies its key roles in cortical neurogenesis and cognitive function. *J Neurosci* 2008;28(27):6983–95.
- [45] Du Y, Du Y, Zhang Y, Huang Z, Fu M, Li J, et al. MKP-1 reduces A β generation and alleviates cognitive impairments in Alzheimer's disease models. *Signal Transduction Targeted Ther* 2019;4:58.
- [46] Burki TJJL. Alzheimer's disease research: the future of BACE inhibitors. *Lancet* 2018;391(10139):2486.